Suitability of vegetation indices derived from Sentinel-2 imagery to model severity of forest damage caused by snow storms. Case study of the Aleppo pine-dominated forests in the Valencian Community

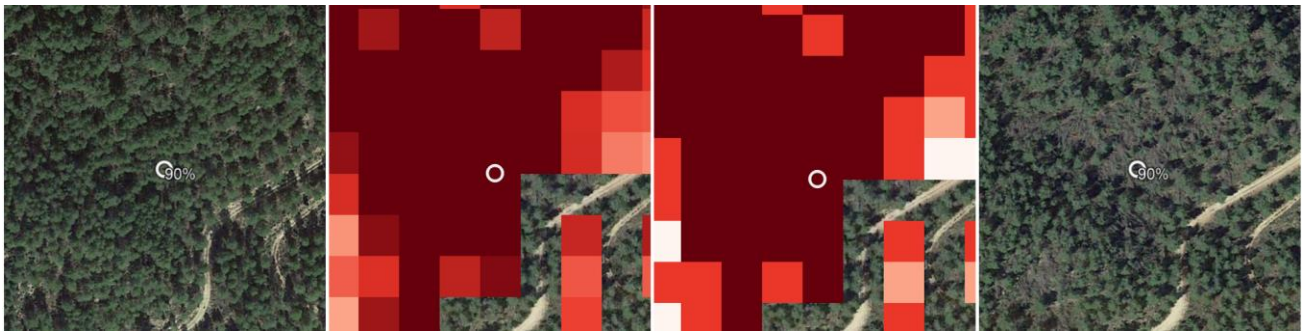

Andrii Khomiuk

02nd of August 2018

Supervised by:

Dr. Santiago Martín-Alcón (Agresta S. Coop.)

Dr. Lluís Coll Mir (University of Lleida / Forest Sciences Centre of Catalonia)

University of Lleida

School of Agrifood and Forestry Science and Engineering

Master thesis:

SUITABILITY OF VEGETATION INDICES DERIVED FROM SENTINEL-2 IMAGERY TO MODEL SEVERITY OF FOREST DAMAGE CAUSED BY SNOW STORMS. CASE STUDY OF THE ALEPPO PINE-DOMINATED FORESTS IN THE VALENCIAN COMMUNITY

Presented by: **Andrii Khomiuk**

Supervised by: **Dr. Santiago Martín-Alcón (Agresta S. Coop.)**

Dr. Lluís Coll Mir (University of Lleida / Forest Sciences Centre of Catalonia)

Abstract

Natural forest disturbances caused by wind or snow storms are reduced to infrequent extreme events in the context of Mediterranean forests. However, when such disturbance events occur they can seriously compromise productive, social and protective functions of forest ecosystem. One of such extreme events occurred in January 2017 on territory of the Valencian Community (Spain). It resulted in a massive conversion of living forest biomass to dead fuel, an increase in fuel bed depth, and decrease in dead fuel moisture. Such outcomes complicate further fire management activities, which are crucial for the Mediterranean region. Taking into account the severity of damage and its large spatial extent, assessment of post-disturbance damage cannot be done manually.

Goal of our study was to compare the performance of different vegetation indices, which are based on data from Sentinel-2 imagery, to quantify negative effects of intensive wind and snow storms on Aleppo pine forests within the territory of Valencian Community. Particular attention was given to building predictive model for quantifying damage level by using a combination of vegetation indices. Latter will find its use for planning post-disturbance restoration activities of the affected forest areas and infrastructures, panning of fire prevention and extinction actions, prioritization of private forest patches (compartments) for subsidizing forest management activities, updating maps of fuel models, etc.

Keywords: vegetation indices; Sentinel-2; storm damage; Random Forest models; Mediterranean region

Acknowledgements

This thesis would never be real without support of people that were around me throughout this tough period of my life.

I am extremely thankful to my supervisors for their encouragements and invaluable support with every aspect of my final work.

Many thanks to José-Antonio Bonet for his patience, wonderful attitude to students and overall dedication to coordinating MEDFOR study program.

Special thank you to all wonderful people, who I met while staying far away from home. Thanks for keeping me on track and never leaving me aside.

Finally, the greatest thank to my family. Мамо, батьку, я б ніколи не досяг теперішніх успіхів без Вас.

Contents

Introduction

Wind and snow storms as disturbances of forest ecosystems

Disturbances are discrete events which change structure of an object, and are caused by a factor external to the level of interest (Pickett, Kolasa, Armesto, & Collins, 1989). In case of ecosystem disturbances, these are events of great importance for the ecosystem and landscape dynamics (e.g. initiation of successions, flow of nutrients, maintainment of biodiversity, etc. (Attiwill, 1994). However, in many forest ecosystems, natural disturbances can seriously compromise the productive and protective function assigned by forest managers at the short term. Proper evaluation and quantification of disturbance events is an important prerequisite for the opportune planning and/or adjustment of management.

White and Pickett (1985) distinguish such major natural disturbances, as fire, wind storms, snow/ice storms, freeze damage, droughts, floods, insect outbreaks, etc. Intensive wind storms are one of the most common disturbance agents for forest ecosystems of Central Europe (Doll, 2000; Schelhaas, Nabuurs, & Schuck, 2003), however they are less abundant on Iberian Peninsula, where this forest disturbance is commonly restricted to the north-west, and the Pyrenees (Castedo-Dorado, Crecente-Campo, Alvarez-Alvarez, & Barrio-Anta, 2009; Martín-Alcón, González-Olabarría, & Coll, 2010). Wind effects on forests can increase notably when occurred after snow storms causing high snow loads over the forest canopy (Nykänen, Peltola, Quine, Kellomäki, & Broadgate, 1997), especially when tree species are not adapted to this situation (i.e. wood of low density and poor resistance, shallow root system, etc.).

Data from global and regional climate models (Donat, Leckebusch, Wild, & Ulbrich, 2011) suggests a decrease in extreme wind speeds over Iberian peninsula during the period 2021-2050. However, during the last years, unusual snow storms followed by strong winds have occurred with certain frequency in the Mediterranean area of the Iberian Peninsula (Llasat, Turco, Quintana-Seguí, & Llasat-Botija, 2014; Martín-Alcón, Gil-Tena, & Cantón, 2017; Martín-Alcón et al., 2010). Such events caused particularly severe effects due to the susceptibility of Mediterranean tree species, which are poorly adapted to snow loads. It has led to a new challenge for the management of the fire-prone Mediterranean forests, since damages caused by wind and snow storms produce important amount of dead biomass, which facilitates and increases severity of the major threat for the Mediterranean ecosystems – wildfires.

Taking into account that wind and snow storms generate partial damage to forest stands, its detection and quantification on large territories may be challenging and time demanding process if done manually on the site. In this case, remote sensing may be perceived as rapid, cost-effective and accurate way to support post-disturbance management and/or restoration, e.g. detection of burn severity after a wildfire (Fernández-Manso, Fernández-Manso, & Quintano, 2016; Mallinis, Mitsopoulos, & Chrysafi, 2018), estimation of defoliation of Scots pine in Poland (Hawryło, Bednarz, Wężyk, & Szostak, 2018), mapping disturbance agents in the US (Schroeder et al., 2017), monitoring deforestation across the tropics (Schultz et al., 2016), assessment of post-hurricane damage in the US (Wang, Qu, Hao, Liu, & Stanturf, 2010), assessment of ice storm damage in forests of southern China (Wu, Wang, Pan, Li, & Huang, 2016), etc.

Remote sensing and algorithms for detection and quantification of wind and snow storm damage

Remote sensing implies obtaining information about object without direct contact with it. Spaceborne satellites facilitate remote sensing of large territories with relatively high resolution and possibility of time series analyses. As of forestry, remote sensing has found its use for analysis of species distribution, forest health, stand structure, overall monitoring of changes over time, etc. (Franklin & Wulder, 2003). As soon as our study concerns the detection of negative effects of storms (e.g. generation of dead biomass through crown breakages, tree uproots, etc.) on large territory, the use of remote sensing is a viable technique to succeed with our goals. Improvement of spatial resolution, frequent revisit times and overall availability (openness) of data significantly eased the acquisition of data and its analysis during recent years. However, multispectral sensors are sensitive to cloud cover which makes the availability of data more limited and dependent on weather conditions. Possible ways to overcome the issue are:

- combination with data from Light Detection and Ranging (LiDAR) sensors, commonly airborne, which, in addition, provide valuable information related to forest structural attributes;
- the use of multispectral sensors with frequent revisit times;
- the use of image composites, which are created based on the cloud-free pixels across certain period of time.

Nowadays, Sentinel 2 stands out among other multispectral satellites due to its open access to the data, high spatial capabilities (resolution up to 10 m) and availability of

bands, which are particularly important for studying vegetation (Ban, Jacob, & Gamba, 2015; Dostálová, Hollaus, Milenković, & Wagner, 2016; Fernández-Manso et al., 2016; Hirschmugl et al., 2017; Verhegghen et al., 2016). With that in mind, our study was based on the data from Sentinel 2 satellite.

Remote sensing produces the raw data in raster format, where each pixel represents a georeferenced measurement value. This raster data can only be used for further analysis after applying necessary preprocessing steps. Particularly, for Sentinel 2 products they may include resampling with constant Ground Sampling Distance (GSD), radiometric and geometric corrections with sub-pixel accuracy (Level 1C), Sen2Cor atmospheric correction (Level 2A), topographic correction, etc. (European Space Agency, 2015).

In a nutshell, change detection using remotely sensed data assumes comparison of raster images taken within particular timeframe. Some changes are obvious when just looking at two images of same landscape in different acquisition time with naked eye. Nonetheless, more precise analysis and comparison is achieved with further image processing in order to enhance "change signals" (Canty, 2009). All methods of such image processing may be distributed within two paradigms: object-based change detection (OBCD) and pixel-based change detection (PBCD). Although OBCD is said to be advantageous over PBCD, latter is much more studied and abundant, when it comes to practical application of methods (G. Chen, Hay, Carvalho, & Wulder, 2012; Hussain, Chen, Cheng, Wei, & Stanley, 2013). Canty (2009) distinguishes such groups of PBCD methods, as:

- Algebraic methods, e.g. subtraction of pixel values, differences in vegetation indices or tasseled cap transforms;
- Postclassification Comparison, e.g. comparison of thematic maps (produced after the classification of satellite images);
- Principal Components Analysis (PCA), e.g. comparison based on scatterplots;
- Multivariate Alteration Detection (MAD), e.g. comparison of scalar images (produced with the introduction of random variable);
- Methods of supervised classification of changes by using machine learning techniques.

Few studies have focused on the damage caused with wind or snow storms on the Iberian Peninsula (Liberato, 2014; Llasat et al., 2014; Montagné-Huck & Brunette, 2018), or its assessment using remote sensing (Bech, Pineda, Rigo, & Aran, 2013; Martín-Alcón et al., 2010). As of today, no operational and validated algorithm for a rapid and accurate

assessment of the post wind or snow storm disturbance was found, particularly in terms of generated dead biomass and changes in forest structure. Nevertheless, there are some valid examples developed in other forest ecosystems, e.g. forest damage assessment after the hurricane in the US (Wang et al., 2010) or after ice storm in China (Wu et al., 2016).

Case of the Valencian Community (17-23 of January 2017)

An intensive winter storm had dramatic consequences on the territory of Valencian Community during a week from 17th till 23rd of January 2017. Atmospheric instability was caused by existence of great amount of cold air within high levels of the atmosphere. On the 19th of January strong winds from West were combined with humid airflow from the East (Núñez Mora, 2017) and produced high level of precipitation. Latter affected almost all territory of the Valencian Community.

The highest intensity of snow storm was recorded on the 19th of January. Both snow and wind storms initially affected provinces of Alicante and southern part of Valencia in the morning, while continuing the movement towards rest of the province of Valencia and, consequently, province of Castellon in the afternoon. On the 20th of January, snow storm progressed in the North direction affecting the interior of the province of Castellon, while leaving provinces of Alicante and Valencia. On the 21st of January, snow storm started to deplete over the Province of Castellon leaving a snow layer of more than 70 cm thick. In general, between 17th and 23rd of January 2017, precipitation (both rain and snow) has exceeded 300 l·m^{-2} in towns within mountainous part of Alicante, while all three provinces of the Valencian Community had maximum precipitation level over 200 l·m^{-2} (Figure 1).

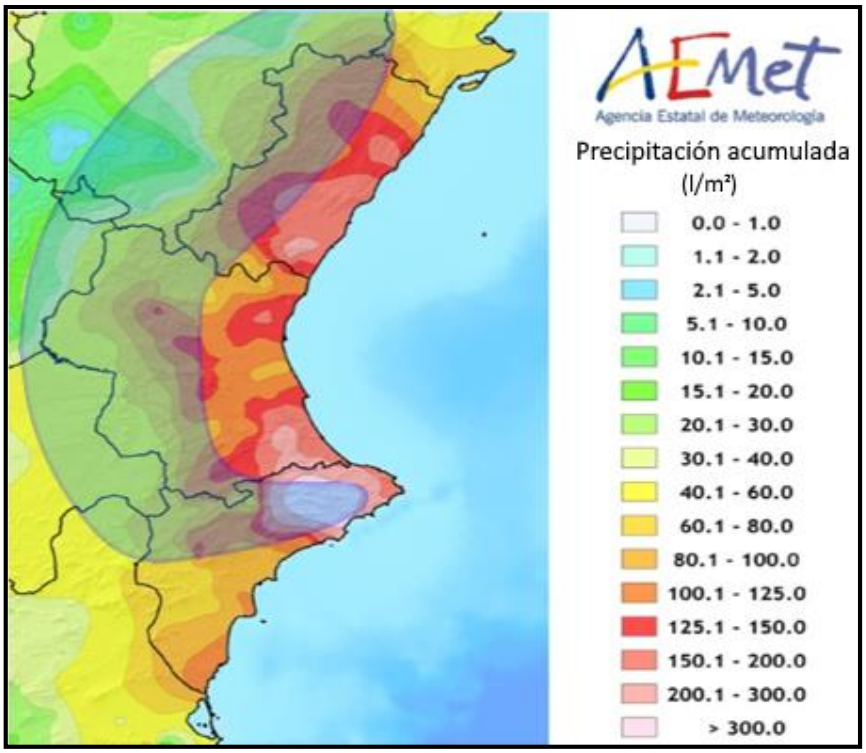

Figure 1. Accumulated rainfall in the Valencian Community during the storm within the period of 17th and the 23rd of January 2017. Shaded area was the most heavily affected by snowfall (modified from Núñez Mora (2017)

Large amount of precipitation in form of snow (up to 70 cm on the treetops) had negative effects on local major tree species, which are not adapted to such conditions, e.g. Aleppo pine (*Pinus halepensis* Miller), maritime pine (*Pinus pinaster* Aiton), holm oak (*Quercus ilex* L.) and cork oak (*Quercus suber* L.). The most obvious consequences of disturbance were seen as breakage of separate branches or whole crowns of trees on large territories.

Soils supplemented with extra humidity due to intense rainfall and occurrence of strong wind storms have facilitated the tree uprooting damage. As a result, thousands of hectares of tree stands were damaged, causing the accumulation of large amount of dead biomass, which is exposed to forest fires, dispersion of forests pests, etc.

Goal and objectives of study

Goal of our study is to compare the performance of different vegetation indices (derived from Sentinel-2 imagery) and to quantify negative effects of intensive wind and snow storms on Aleppo pine forests within the territory of Valencian Community.

Specific objectives are:

1. Identify possible indicators and methods for detecting damage produced by wind and snow storms with the help of remote sensing;
2. Compare the performance of different vegetation indices to quantify the severity of damage (as percentage of dead biomass), relating the values of these indices with damage data from field inventory;
3. Build a predictive model for quantifying damage level using a combination of vegetation indices.

Obtained information will find its use for:

- Planning post-disturbance restoration activities of the affected forest areas and infrastructures, e.g. forest roads, pathways, etc.;
- Planning of fire prevention and extinction actions;
- Prioritization of private forest patches (compartments) for subsidizing forest management activities;
- Updating maps of fuel models, etc.

Material and methods

Study area

Valencian Community is situated in the eastern part of the Iberian Peninsula and has a direct access to the Mediterranean Sea (Figure 2).

Figure 2. Location of the study area (orange color) within territory of Spain. Base map: Google satellite imagery

Relief is uneven and includes both plain and mountainous areas, though latter is dominant. Altitude varies from sea level to 1839 m a.s.l. Mountain ranges on the north of region are part of the Iberian System and on the south – part of the Prebaetic System. Complex typography, i.e. steep hills and wide range of altitude, together with proximity to the Mediterranean Sea contribute to the spatial variation of local climatic conditions. Typical Mediterranean climate with hot and dry summer and mild and humid winter prevails in the territory of Valencian Community. Snow damages to local forests are rare and mostly localized within mountainous areas.

Tree species composition is dominated by such conifers, as Aleppo pine (*Pinus halepensis* Mill.) and maritime pine (*Pinus pinaster* Aiton). Aleppo pine is main species in the mountainous areas covering over 4 687 km^2 (MAGRAMA, 2015). Although Aleppo pine is well-adapted to forest fires, droughts and wind storms, it is rather susceptible to the snow damage over its large accumulation on canopy.

A quick survey was established right after the snow storm event of January 2017 by the Valencian Forestry Service. It testified that stands with Aleppo pine as dominant tree species were the most influenced with snow damage. However, precise information about the damage severity was not available at the time of the survey.

Processing of Sentinel-2 satellite imagery

Sentinel-2 multi-spectral instrument provides data within 13 spectral channels at varying spatial resolution (Table 1).

Band	Central wavelength (nm)	Spatial resolution, m	Bandwidth (nm)
1 – Coastal aerosol	443	60	20
2 – Blue	490	10	65
3 – Green	560	10	35
4 – Red	665	10	30
5 – Vegetation Red Edge	705	20	15
6 – Vegetation Red Edge	740	20	15
7 – Vegetation Red Edge	783	20	20
8 – NIR	842	10	115
8A – Narrow NIR	865	20	20
9 – Water vapor	945	60	20
10 – SWIR – Cirrus	1375	60	30
11 – SWIR	1610	20	90
12 – SWIR	2190	20	180

Table 1. Summary of available spatial resolution bands on Sentinel-2 (adapted from European Space Agency (2015)

Level-1C Sentinel-2 products were acquired from the ESA Sentinel Data Hub. Seven scenes (30TYL, 30TXK, 30TYK, 30SXJ, 30TYJ, 30SXH and 30SYH) were enough to cover whole study area (Figure 3).

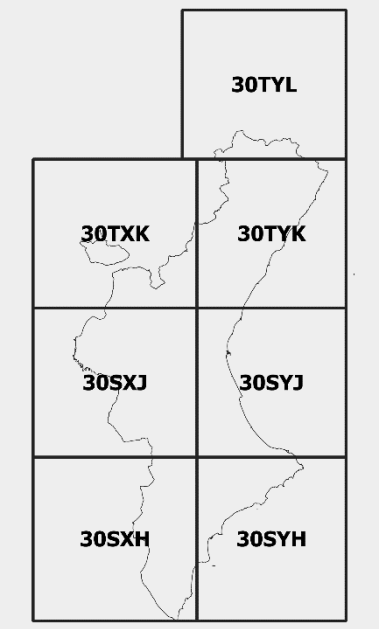

Figure 3. Sentinel-2 scenes, which were used in the study

Each scene was obtained at least in two variants (prior storm disturbance of January 2017 and post disturbance) with the criteria of less than 30% of clouds and highest sun elevation in order to minimize post-processing. Eventually, 9 dates for the pre-disturbance series (1/05/2016, 26/05/2016, 14/07/2016, 20/06/2016, 30/06/2016, 10/07/2016, 30/07/2016, 10/08/2016, 19/08/2016) and 10 dates for the post-disturbance series (6/05/2017, 16/05/2017, 26/05/2017, 15/06/2017, 5/07/2017, 10/07/2017, 25/07/2017, 30/07/2017, 4/08/2017, 14/08/2017) were used for further processing and creation of 2 mosaic images. Our study was based on bands B2, B3, B4, B5, B6, B7, B8, B8A, B11, B12. These bands incorporate wavelengths, which were proved to describe vegetation status in other researches. Spatial resolution of these bands was homogenized to 20 m.

Further processing included:

1. Sen2Cor atmospheric correction to get to the Level-2A product (European Space Agency, 2017);
2. Topographic correction with the C correction model (Riano, Chuvieco, Salas, & Aguado, 2003) based on the DEM derived from LiDAR data (Spanish Ministry of Public Works and Transport, 2018);
3. Creation of a spatially continuous cloud-free composite image according to the maximum-NDVI-value composite method (Holben, 1986; Ramoino, Tutunaru, Pera, & Arino, 2017) for both pre- and post-disturbance periods

Processing was done using RStudio software incorporating R 3.5.0 (RStudio Team, 2016) and Sentinel-2 Toolbox 6.0.1 (European Space Agency, 2017). Each image was processed independently and without the normalization of time series.

Field inventory

Collection of field data was designed and done on a set of 60 sample plots by employees of Agresta S. Coop. in December 2017 (Martín-Alcón et al., 2017). Sample plots (Figure 4) were located using a stratified random sampling.

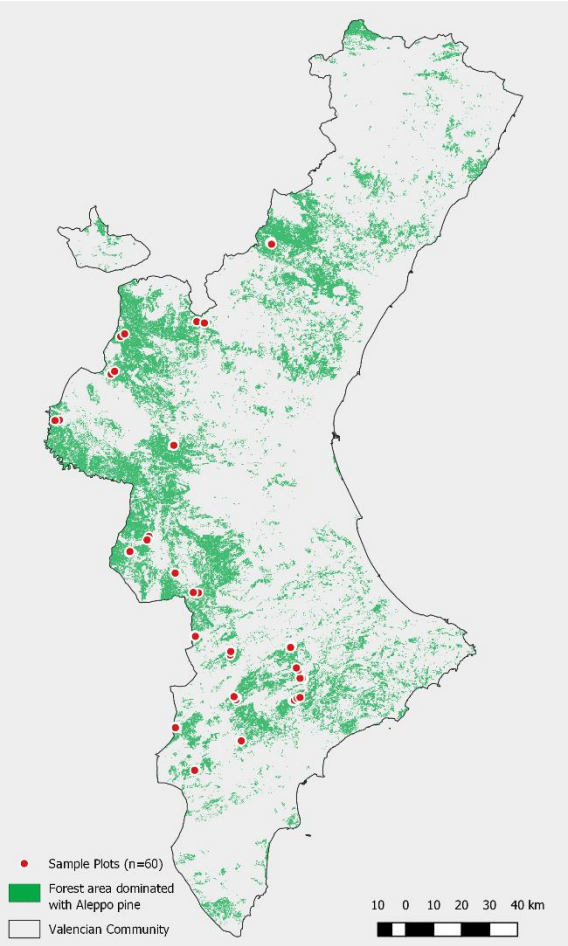

Figure 4. Distribution of sample plots within the study area

Strata were based on:

- the outcomes of applying the iteratively reweighted multivariate alteration detection (IR-MAD) (Nielsen, 2007) on the pre- and post-disturbance image composites. Specifically, the IR-MAD chi-square indicator of probability of change has been reclassified into four classes: no change, low probability, medium probability, high probability. The change itself was assumed to be caused with storm damage due to the fact that storm disturbance was the only event resulting in extensive tree mortality within the analyzed period;
- distribution map of Aleppo pine stands within public forests of Valencian Community, obtained by intersection of Aleppo pine-dominated stands (MAGRAMA, 2015) with

cartography of public forests under management of Valencian Forestry Service (GVA, 2017);

- accessibility (distance to forest road or pathway higher than 50 m and lower than 150 m).

Fifteen plots were placed within each of 4 levels of probability of change identified by IR-MAD. Coordinates of the sample plot centers were set as a center of a 20-meter pixel, identified in the field with a Trimble Geo 7X GPS. In order to avoid small-scale variation that could negatively affect further analyses, sample plot was placed within in a pixel if it was surrounded by 8 pixels of the same level of change probability. Sample plot itself represented a circle of 10-meter radius. The data was collected in a form generated using CyberTracker software (CyberTracker Conservation, 2013) and included following information:

- main species and its share within all species that were present on the plot;
- secondary species and its share within all species that were present on the plot;
- percentage of dead biomass from the tree canopy with respect to the pre-disturbance total biomass (estimated);
- type(s) of damage observed (i.e., none, broken branches, truncated stems and / or uprooted trees);
- the most probable cause of them (snow, wind, biotic and management interventions).

Dead biomass was assessed visually in 5% classes and separately for the main and secondary species. Total damage (i.e., total percentage of dead biomass) was estimated as the sum of the percentage of dead biomass observed for each species multiplied by the fraction species' share within all species that were present on the sample plot. In the case of plots which clearly showed the anthropogenic source of damage, they should have been discarded and substituted. However, such cases didn't happen.

Vegetation Indices

Vegetation indices (VIs) are perceived as simple approaches to extract certain information from the products of remote sensing. VIs are computed mathematically without the influence of subjectivity on the state of study area, e.g. climatic conditions, available vegetation, etc. Particularly in environmental studies VIs are widely used to estimate abundance of vegetation biomass, monitor stress events, biophysical parameters of vegetation, etc. (J. M. Chen, 1996; Fernández-Manso et al., 2016; A. Huete et al., 2002; Hunt et al., 2013; Mašková, Zemek, & Květ, 2008).

In this study we compared performance of 17 VIs, that are widely used for monitoring of green vegetation, in regard to their validity to quantify the level of snow storm damage observed in Aleppo pine forests on territory of Valencian Community. Each VI was calculated based on the pre- and post-disturbance values of pixels, which represent location of sample plots with measured severity of damage. Afterwards, the relative difference between pre- and post-disturbance values of each VI was derived following the same approach as proposed in Miller & Thode (2007):

$$RdVI=\left(\frac{preVI-postVI}{\sqrt{\left|\frac{preVI}{1000}\right|}}\right)$$

All selected VIs are briefly described in the following subsections.

Enhanced Vegetation Indices (EVI, EVI2)

EVI (A. Huete, 1997) was developed to improve the derived calculation results in high biomass regions, where the leaf area index (LAI) is high. Its mathematical rational is based on introduction of the blue visible band and extra coefficients (gain factor, canopy background adjustment and aerosol resistance term).

$$EVI=2.5\times\frac{B08\_nir-B04\_red}{B08\_nir+6\times B04\_red-7.5\times B02\_blue+1}$$

Values of EVI range from -1 to 1. Healthy vegetation generally is represented with values within 0.20 and 0.80.

EVI2 (Jiang, Huete, Didan, & Miura, 2008) was developed and evaluated as a 2-band index and equivalent to the 3-band EVI.

$$EVI2=2.5\times\frac{B08\_nir-B04\_red}{B08\_nir+2.4\times B04\_red+1}$$

Values of EVI2 range from -1 to 1 and the difference from EVI is within ±0.02.

Green Normalized Difference Vegetation Index (GNDVI)

GNDVI (A. A. Gitelson & Merzlyak, 1998) was developed as an alternative to the NDVI.

$$GNDVI=\frac{B08\_nir-B03\_green}{B08\_nir+B03\_green}$$

GNDVI ranges from -1 to 1. It is more sensitive to the concentration of chlorophyll and has wider dynamic range.

Green Ratio Vegetation Index (GRVI)

GRVI (Sripada, Heiniger, White, & Meijer, 2006) is sensitive to photosynthetic rates in forest canopies, which makes it useful to determine any changes that influence leaf pigments.

$$GRVI=\frac{B08\_nir}{B03\_green}$$

Chlorophyll Absorption Ratio Indices (MCARI, TCARI)

Modified Chlorophyll Absorption Ratio Index (MCARI) and Transformed Chlorophyll Absorption Reflectance Index (TCARI) were developed as indicators of relative abundance of chlorophyll (Daughtry, 2000; Haboudane, Miller, Pattey, Zarco-Tejada, & Strachan, 2004).

$$MCARI=\left[\begin{matrix}(B05\_rededge-B04\_red)-\\0.2\times(B05\_rededge-B03\_green)\end{matrix}\right]\times\left(\frac{B05\_rededge}{B04\_red}\right)$$

$$TCARI=3\times\left[(B05\_rededge-B04\_red)-0.2\times(B05\_rededge-B03\_green)\times\left(\frac{B05\_rededge}{B04\_red}\right)\right]$$

However, results of these indices may be influenced by the reflectance of underlying soil in sparse vegetation cover.

Moisture Stress Index (MSI)

MSI was developed by Hunt Jr. & Rock (1989) to detect changes in leaf water content using reflectance in the near-infrared and middle-infrared wavelengths (MWIR). It is commonly used for the canopy stress analysis and productivity prediction (Welikhe, Quansah, Fall, & McElhenney, 2017).

$$MSI=\frac{B11\_swir}{B08\_nir}$$

Values of MSI range from 0 to more than 3. Green vegetation is detected within 0.4 to 2. The higher the value of MSI, the more stressed the vegetation is in the context of water availability. In our study we used an available SWIR band on the Sentinel-2a instead of MWIR.

Modified Simple Ratio NIR/RED (MSRNir/Red)

MSRNir/Red was initially developed and evaluated to retrieve biophysical parameters of boreal forests (J. M. Chen, 1996).

$$MSR = \frac{\left(\frac{B08\_nir}{B04\_red}\right) - 1}{\sqrt{\left(\frac{B08\_nir}{B04\_red}\right) + 1}}$$

This VI is non-linear and is less sensitive to canopy optical and geometrical properties.

Normalized Difference Infrared Index (NDII)

NDII (Hardisky, Klemas, & Smart, 1983) was developed to estimate the vegetation water content based on difference of light reflectance in NIR and SWIR wavelengths.

$$NDII = \frac{B08\_nir - B11\_swir}{B08\_nir + B11\_swir}$$

Values of NDII range from -1 to 1 and green vegetation is detected within values from 0.02 to 0.6. The higher the value, the higher is the water content. It is widely used monitoring forest canopy and detection of vegetation stress.

Normalized Difference Vegetation Index (NDVI)

NDVI (Rouse, Haas, Schell, & Deering, 1974) is historically the first and the most used VI for estimation of vegetation biomass, detection of dominant species, etc. Mathematically, it is a ratio between the red and NIR bands:

$$NDVI = \frac{B08\_nir - B04\_red}{B08\_nir + B04\_red}$$

Resulting values vary within a range from -1 to 1 and the higher the value, the more abundant green biomass is within a pixel. NDVI is able to separate vegetation from other surfaces because of chlorophyll light absorption in the red wavelength and its reflection in the NIR wavelength (Tucker, 1979). This VI is capable to reduce many sources noise from cloud shadows, topographic variations or basic illumination differences. However, NDVI is less informative when it comes to separating very dense canopy from dense canopy (Wang et al., 2010).

Normalized Difference Red-Edge (NDREI)

NDREI (Barnes et al., 2000) was developed as a stress-detection VI based on the red-edge band, which is capable of penetrating the leaf better than the red band. According to Eitel et al. (2011), NDREI is capable to detect stress event better than NDVI or GNDVI.

$$\text{NDREI}=\frac{\text{B08\_nir-B05\_rededge}}{\text{B08\_nir+B05\_rededge}}$$

Values of this index range from -1 to 1 and green vegetation is present within 0.2 and 0.9. NDREI improves the sensitivity of results to small changes in forest canopy, e.g. creation of minor gaps.

Red Edge Normalized Difference Vegetation Index (RENDVI)

RENDVI (A. Gitelson & Merzlyak, 1994) was developed as a modification of traditional NDVI. Instead of main absorption and reflectance peaks it uses bands along the red edge. Latter improves the sensitivity towards small changes, e.g. gap creation.

$$\text{RENDVI}=\frac{\text{B06\_rededge-B05\_rededge}}{\text{B06\_rededge+B05\_rededge}}$$

Soil Adjusted Vegetation Indices (SAVI, MSAVI2, OSAVI)

SAVI (A. R. Huete, 1988) was developed to remove the soil background effect in areas, where vegetative cover is sparse. Its mathematical representation incorporates a soil brightness correction factor 0.5. However, such correction lowers overall sensitivity of this VI (at least, compared to the NDVI).

$$\text{SAVI}=1.5\times\frac{\text{B08\_nir-B04\_red}}{\text{N08\_nir+B04\_red+0.5}}$$

Values of SAVI vary from -1 to 1. Lower values represent lower vegetation cover.

Modified Soil Adjusted Vegetation Index (Qi, Chehbouni, Huete, Kerr, & Sorooshian, 1994) reduces the soil noise and increases the dynamic range of green vegetation.

$$MSAVI2=\frac{2\times B08\_nir+1-\sqrt{\left(2\times B08\_nir+1\right)^{2}-8\times\left(B08\_nir-B04\_red\right)}}{2}$$

Optimized Soil Adjusted Vegetation Index (Rondeaux, Steven, & Baret, 1996) was developed as an improved version of SAVI. It used a value of 0.16 for the canopy background adjustment.

$$OSAVI=\frac{\left(B08\_nir-B04\_red\right)}{\left(B08\_nir+B04\_red+0.16\right)}$$

OSAVI is particularly useful for areas with relatively sparse vegetation cover and, as a result, visible soil.

Triangular vegetation index (TVI)

TVI (Broge & Leblanc, 2001) incorporates NIR, green and red wavelengths, which are sensitive to both chlorophyll content and leaf area index. It is calculated as the area of hypothetical triangle in spectral space. The sensitivity of this index increases with the density of vegetation cover.

$$TVI=0.5\times\left[\begin{array}{l}120\times\left(B08\_nir-B03\_green\right)-\\-200\left(B04\_red-B03\_green\right)\end{array}\right]$$

It is based on the fact that both chlorophyll absorption causing a decrease of red reflectance and leaf tissue abundance causing increased NIR reflectance will increase the total area of the triangle.

Development of models

Random Forest regression and classification models for prediction the severity of damage were based on vegetation indices as predictors. Regression model used continuous values of total damage as dependent variable. A categorical variable was derived out of total

damage values and was based on the quartiles of distribution as breaking points (Table 2). Damage severity categories were used as response variables for classification model.

Total damage, %	Damage severity category
< 2	0
2 ≤ x < 10	1
10 ≤ x < 35	2
≥ 35	3

Table 2. Calculation of damage severity categories based on numerical values

Initial variable selection was done using RF and, specifically, VSURF R package (Genuer, Poggi, & Malot, 2015). The algorithm of VSURF incorporates three steps: tresholding (getting rid of irrelevant variables), interpretation (selection of variables related to the response for interpretation purpose) and prediction (clearing redundant predictors). VSURF was applied separately for regression and classification models.

Random Forest (RF) and its corresponding function R function (Breiman, 2001; Liaw & Wiener, 2002) was used as a machine learning method for creating regression and classification models in RStudio software (RStudio Team, 2016). RF algorithm is a nonlinear technique to predict values by aggregating either classification or regression trees each built using a different random sample of data and choosing splits of the trees from set of vegetation indices as predictors that are randomly chosen from the node (Breiman, 2001). Values of parameters "mtry", "ntree" and "nodesize" were set to defaults. Variable importance was analyzed with plotting mean square error (%IncMSE).

Model validation was performed using rf.crossValidation function of rfUtilities R package (Evans & Murphy, 2018). Latter is capable of implementing a permutation test cross-validation for both classification and regression RF models. For classification model it outputs the confusion matrix (for the analysis of cross-classification error), OOB error, Kappa statistic. For regression models output is different due to their different nature and consists of mean square error, percent variance explained and root mean square error (RMSE) between the response variable and predicted model. Arguments for proportion data withhold and number of cross-validations were set to its defaults – 0.1 and 99 respectively.

Generation of damage severity raster maps

Raster images containing values of relative difference for each VI were generated based on pre- and post-disturbance Sentinel-2 composite images. Following calculations involved

only those VIs, which were used as predictors for either classification or regression RF model. Outputs of RF models were later used to generate final raster files of predicted damage in absolute values (based on the regression model) and damage severity categories (based on the classification model). Whole process of generation of raster files involved "raster" R package (Hijmans, 2017). Further visualization of results was done in QGIS software of version 3.2.0 (QGIS Development Team, 2018).

Results

Calculation of VIs

All VIs were calculated based on values of pixels of pre- and post-disturbance composite Sentinel-2 images with the correspondence to location of sample plots. Relative difference of each VI was plotted against values of total damage obtained from the field data (Figure 5) to get an initial overview on the performance of VIs.

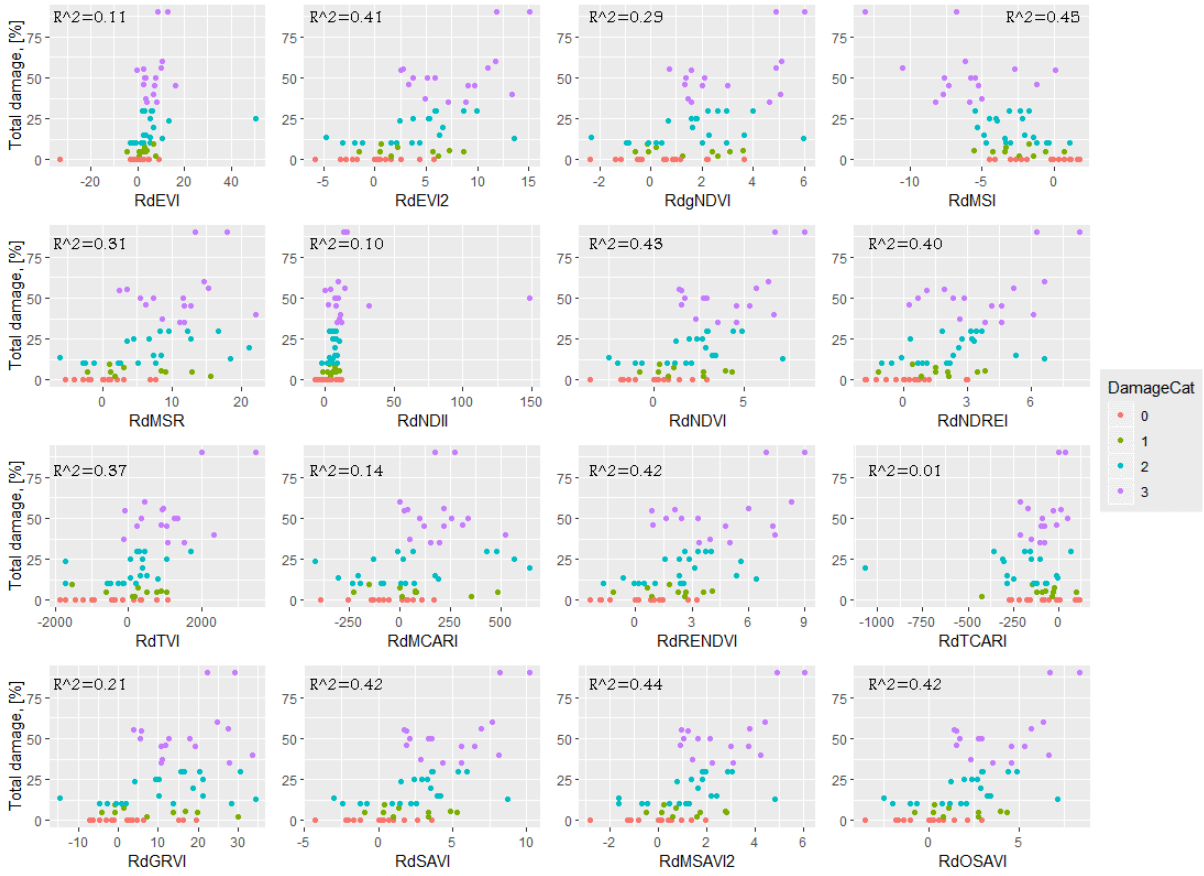

Figure 5. Scatterplots of regression between total damage observed in the field plots, and the relative difference of Vis. Colors correspond to damage categories as defined in Table 2.

None of the VIs showed a clear linear relationship. Although indices TCARI, MCARI, EVI and GRVI performed worse than other, they were still included into further variable selection process to avoid subjective handpicking of predictors.

Variable selection

Variables selection using Random Forests (VSURF) resulted in 3 predictors for classification model: RdMSI, RdNDII, RdSAVI. As of regression model, VSURF selected 2 VIs as predictors: RdMSI, RdNDVI. Results of variable screening is shown in Table 3.

	Thresholding step	Interpretation step	Prediction step
Classification RF model	13	5	3
	RdMSI, RdNDII, RdNDVI, RdOSAVI, RdSAVI, RdMSR, RdTVI, RdEVI2, RdRENDVI, RdMSAVI2, RdNDREI, RdTCARI, RdEVI	RdMSI, RdNDII, RdNDVI, RdOSAVI, RdSAVI	RdMSI, RdNDII, RdSAVI
Regression RF model	16	2	2
	RdMSI, RdNDVI, RdEVI2, RdSAVI, RdOSAVI, RdMSAVI2, RdMSR, RdNDII, RdTVI, RdRENDVI, RdGNDVI, RdTCARI, RdNDREI, RdGRVI, RdEVI, RdMCARI	RdMSI, RdNDVI	RdMSI, RdNDVI

Table 3. Screening of predictors at each step of VSURF process

Relative differences of such indices as MSR, EVI, EVI2, TVI, GNDVI, NDREI, MSAVI2, RENDVI, TCARI, GRVI and MCARI haven't passed through the initial step of VSURF algorithm.

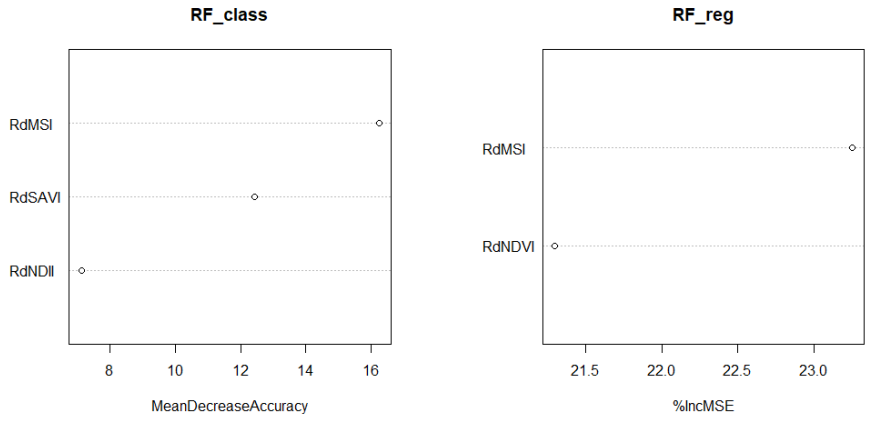

Figure 6. Variable importance plots for classification and regression Random Forest models

In case of MSI, its relative difference was the most important predictor for both classification and regression models (Figure 6).

Random Forest models cross-validation

Cross-validation of the classification Random Forest model resulted in the following confusion matrix (Table 4).

	0	1	2	3	Classification error
0	8	3	3	1	0.4666667
1	4	0	4	1	1.0000000
2	4	3	12	1	0.4000000
3	2	0	4	10	0.3750000

Table 4. Confusion matrix for classification model

Classification RF model was able to correctly classify 50% values (OOB Error), while Kappa statistic is equal to 0.31. The classification error decreased with the increase of damage severity. Latter suggests that classification model performs better with classifying severe abrupt changes, when compared to minor changes.

As of the regression RF model, it explained 44.7% of variance with the median cross-validation RMSE equal to 15.70199. Scatterplot of predicted values of total damage and those observed on sample plots is shown on Figure 7.

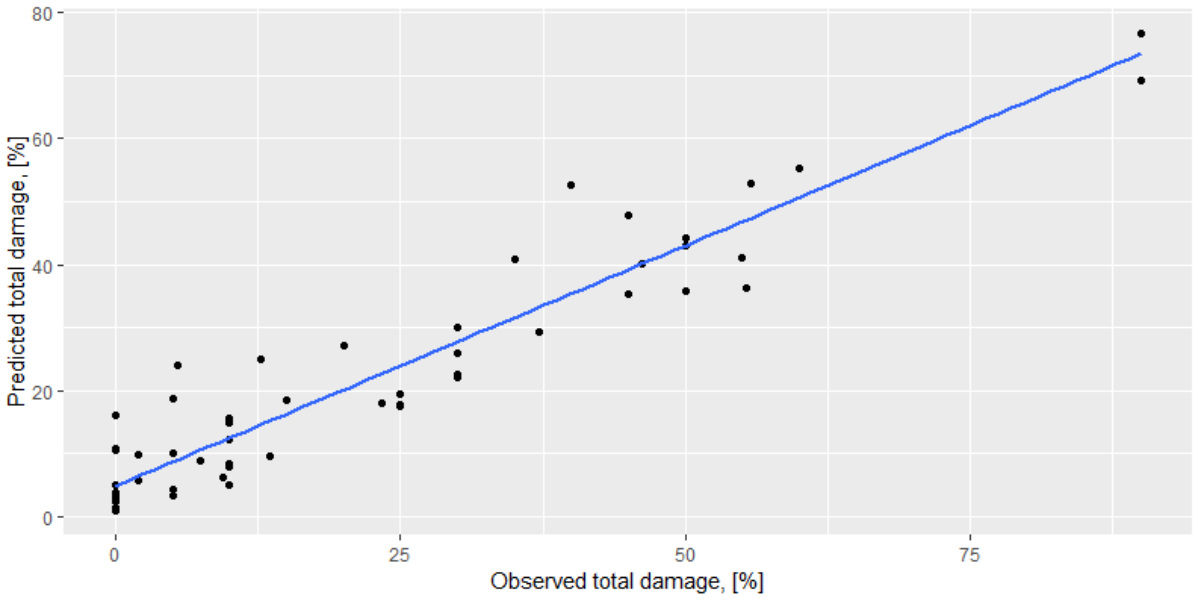

Figure 7. Scatterplot of total damage severity observed on sample plots and predicted by the regression Random Forest model

Damage severity maps

RF models were used to predict the damage severity for the whole study area. For classification model raster map resulted in damage categories (Figure 8a), while regression model – in percentage values of damage severity (Figure 8b).

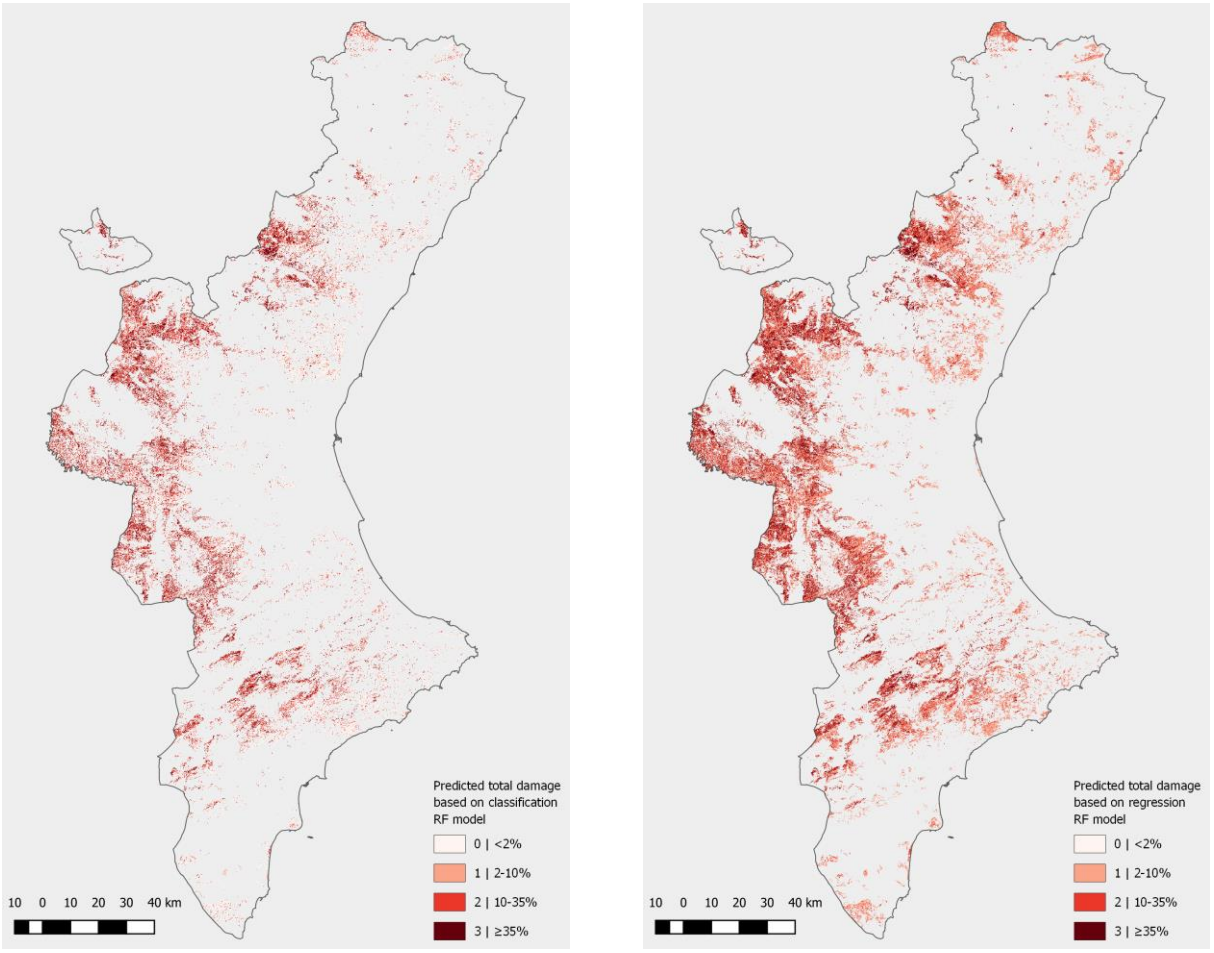

A B

Figure 8. Maps of predicted snow storm damage severity within the study area: A – predicted by classification RF model; B – predicted by regression RF model. Output values of the regression RF model were reclassified using same break points as damage severity category (Table 2) for illustration purpose

Distribution of pixels (Figure 9) shows difference in the output of both models within groups of minor damage. Eventually, classification RF model was able to distinguish the undamaged areas better, then regression model (Figure 8 and 10).

Regression model resulted in classifying the undamaged areas as those with minor damage (up to 10%), and, consequently, overestimating the overall area of predicted damage. In the case of classification model, it tended to underestimate the low-damaged area, what has also been shown within the confusion matrix (Table 4).

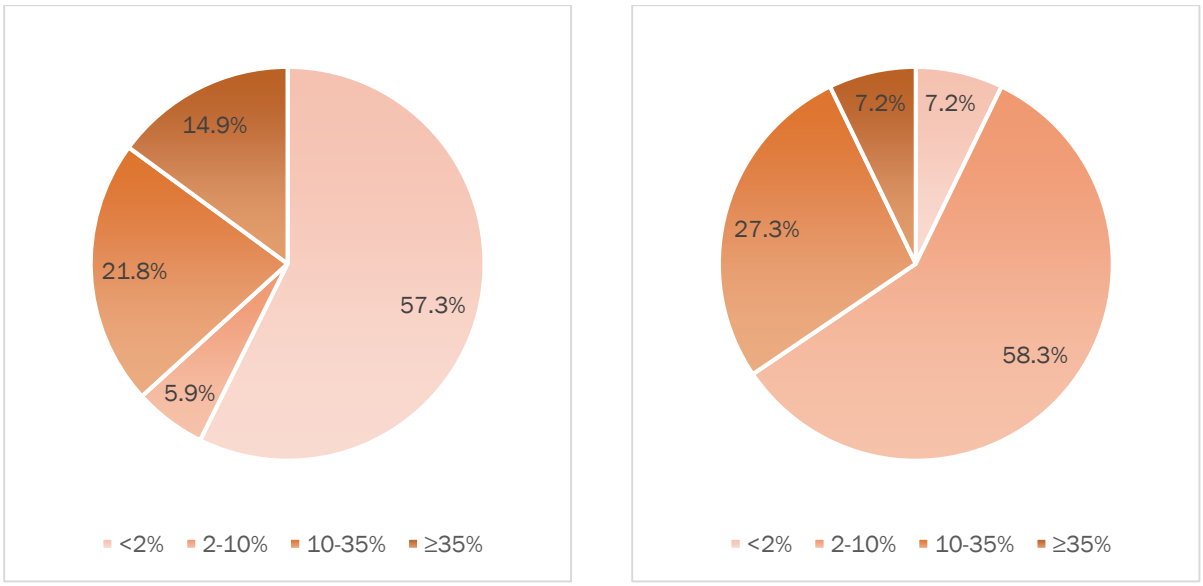

A B

Figure 9. Distribution of pixels within categories of total damage severity: A – predicted by classification RF model; B – predicted by regression RF model. Output values of the regression RF model were reclassified using same break points as damage severity category (see Table 2) for illustration purpose

Regarding areas having medium to high damage severities, both models seem to perform similarly, though regression RF model may underestimate damage severity in highly damaged areas. Latter corresponds to the result of plotting observed damage on sample plots against predicted damage by regression RF model (Figure 7).

Discussion

Importance of VIs as variables

In our study we have tested 16 VIs, which can be calculated based on data from Sentinel-2 imagery: Enhanced Vegetation Indices (EVI and EVI2), Green Normalized Difference Vegetation Index (GNDVI), Green Ratio Vegetation Index (GRVI), Modified Chlorophyll Absorption Ratio Index (MCARI). Moisture Stress Index (MSI), Modified Simple Ratio NIR/RED (MSRNir/Red), Normalized Difference Infrared Index (NDII), Normalized Difference Vegetation Index (NDVI), Normalized Difference Red-Edge Index (NDREI), Red-Edge Normalized Difference Vegetation Index (RENDVI), Soil Adjusted Vegetation Index (SAVI), Modified Soil Adjusted Vegetation Index (MSAVI2), Optimized Soil Adjusted Vegetation Index (OSAVI), Transformed Chlorophyll Absorption Reflectance Index (TCARI), Triangular Vegetation Index (TVI). All these VIs showed a potential to facilitate the modelling of damage severity of the Aleppo pine tree stands, which were influenced by the wind- and snow-storm of January 2017.

As a proxy of change we used the relative difference between pre- and post-disturbance values of VIs, which has been elaborated for Normalized Burn Ratio (NBR) by Miller & Thode (2007). While values of the coefficient of determination for VIs TCARI, MCARI, EVI and GRVI were the lowest, all indices were included in further VSURF algorithm.

According to VSURF, relative difference between values of such indices as MSI, NDVI, NDII and SAVI successfully quantify loss of vegetation cover after wind- and storm damage in January 2017. These indices are based on red, NIR and SWIR wavelengths and are less sensitive to atmospheric contamination.

Performance of RF models and feasibility of mapping results

No operational and validated algorithm to assess the post wind or snow storm damage affecting forested area on Iberian Peninsula was found within available to us sources of information. With that in mind, we cannot compare performance of our models to similar studies in the Mediterranean region.

In general, both RF models predicted damage severity with moderate accuracy (Figure 10). Prediction of low severity damage (up to 10%) was the least accurate. Particularly, classification model was able to distinguish damage in the range from 2% to 10% better than regression RF model. At the same time, accuracy of models' performance increased substantially with the increased severity of damage. Both models resulted in similar and close-to-observed values while predicting abrupt changes in vegetation cover. The reason for that could be spatial resolution of input imagery. In case of Sentinel-2 and, particularly, our study, it was homogenized to 20 m. Such size of pixel may be too large, when it comes to assessment of low-severity changes in reflectance values.

We can also conclude that models' performance was in the range observed in studies using Sentinel-2 imagery to assess the severity of other forest disturbances. For example, Hawryło et al., (2018) reported R^2 values for RF regression model of 0.57 and RMSE of 11.9, and overall accuracies of two-class RF classification model of 75%.

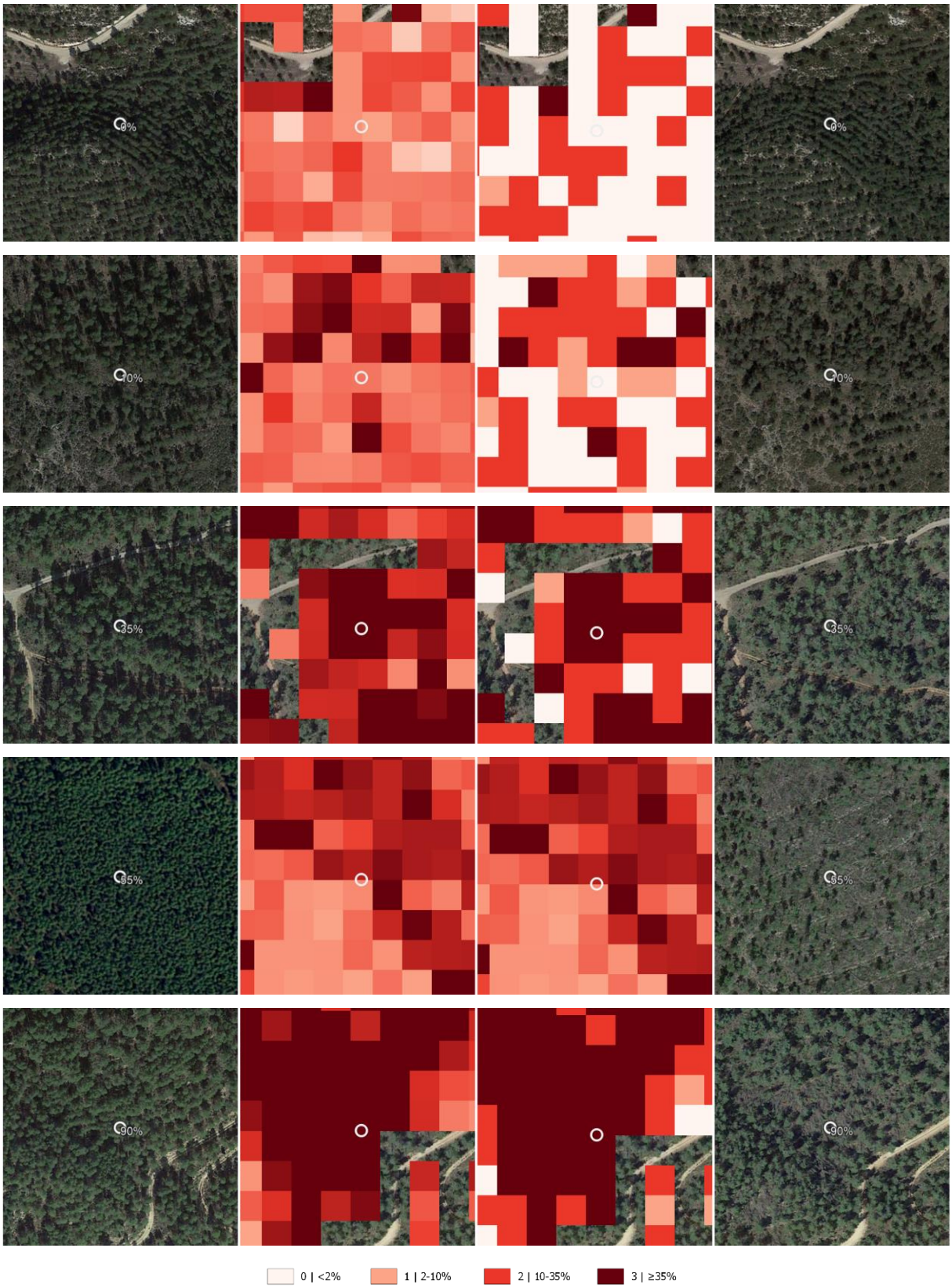

Figure 10. Comparison of regression and classification RF models in predicting post wind- and snow-storm damage severity, compared to observed data from sample plots (from left to right): true-color image prior to disturbance (adapted from timeline of Google Earth Pro, (2018); result of regression model; result of classification model; true-color image after disturbance (adapted from timeline of Google Earth Pro, (2018). Levels of damage severity compared (from top to bottom): 0%; 10%; 35%; 55%; 90%. Circles in the middle of images represent center of sample plots.

The high extent and variability of study area compared to works, which assess other forest disturbances, may have hindered obtaining more accurate models. Moreover, the consideration of four classes of damage severity in order to make a detailed assessment, may have impoverished the overall accuracy of classification RF model. Looking at our results, an alternative method combining the strengths of both regression and classification may be proposed. It would consist on linking two models, first a two-class classification model for damage detection (i.e., damaged/undamaged), later a regression RF to predict damage severity in damaged areas.

In general, the use of remote sensing in general and Sentinel-2 products in particular appeared to be time- and cost-efficient approach to assess post-disturbance damage on a territory of the Valencian Community.

Conclusions

Our study contributed to the development of a new approach for identifying and classifying forested areas, which had been influenced by wind or storm damage. We discovered 16 different vegetation indices and calculated them based on the Sentinel-2 imagery. This allowed us to compare their performance in assessment and quantification of damage severity caused by wind- and snow storm on territory of the Valencian Community (Spain) in January 2017.

Application of the Random Forest machine learning technique helped us to distinguish 4 vegetation indices, relative differences of which were the most valuable in modelling the damage severity: Moisture Stress Index (MSI), Normalized Difference Vegetation Index (NDVI), Normalized Difference Infrared Index (NDII) and Soil Adjusted Vegetation Index (SAVI).

Relative differences of discovered vegetation indices' values were used to build two predictive Random Forest models. First (classification) model used pre-disturbance and post-disturbance values of MSI, SAVI and NDII to predict 4 different categories of damage severity. Second (regression) model was based on relative differences between pre-disturbance and post-disturbance values of MSI and NDVI to predict continuous numerical values of damage severity. Obtained results have been validated with the data from 60 sample plots in forests. Both models predicted damage severity with moderate accuracy: neither of two was able to perform well in modelling damage of 10% or less; but both have

predicted abrupt changes in vegetation cover (damage severity of 35% and more) more precisely. Such outcome may be caused by a spatial resolution of Sentinel-2 products, which was homogenized to 20 m in order to correctly calculate vegetation indices. Such size of pixel may be too large to detect changes in the reflection values, which correspond to the low severity of damage.

Further research, e.g. comparison with other available sources of satellite images, broadening set of predictors, extending the set of sample plots, etc., may improve the algorithm of forest damage assessment and commit to further development of efficient and precise methods of modelling effects of natural disturbances.

References

Attiwill, P. M. (1994). The disturbance of forest ecosystems: the ecological basis for conservative management. *Forest Ecology and Management*, *63*(2–3), 247–300. https://doi.org/10.1016/0378-1127(94)90114-7

Ban, Y., Jacob, A., & Gamba, P. (2015). Spaceborne SAR data for global urban mapping at 30m resolution using a robust urban extractor. *ISPRS Journal of Photogrammetry and Remote Sensing*, *103*, 28–37. https://doi.org/10.1016/j.isprsjprs.2014.08.004

Barnes, E. M., Clarke, T. R., Richards, S. E., Colaizzi, P. D., Haberl, J., Kostrzewski, M., … Moran, M. S. (2000). Coincident Detection of Crop Water Stress, Nitrogen Status and Canopy Density Using Ground Based Multispectral Data. In *In Proceedings of the Fifth International Conference on Precision Agriculture*.

Bech, J., Pineda, N., Rigo, T., & Aran, M. (2013). Remote sensing analysis of a Mediterranean thundersnow and low-altitude heavy snowfall event. *Atmospheric Research*, *123*, 305–322. https://doi.org/10.1016/j.atmosres.2012.06.021

Breiman, L. (2001). Random Forests. *Machine Learning*, *45*(1), 5–32. https://doi.org/10.1023/A:1010933404324

Broge, N. ., & Leblanc, E. (2001). Comparing prediction power and stability of broadband and hyperspectral vegetation indices for estimation of green leaf area index and canopy chlorophyll density. *Remote Sensing of Environment*, *76*(2), 156–172. https://doi.org/10.1016/S0034-4257(00)00197-8

Canty, M. J. (2009). *Image Analysis, Classification, and Change Detection in Remote Sensing: Second Edition* (2nd ed.). Boca Raton: CRC Press.

Castedo-Dorado, F., Crecente-Campo, F., Alvarez-Alvarez, P., & Barrio-Anta, M. (2009). Development of a stand density management diagram for radiata pine stands including assessment of stand stability. *Forestry*, *82*(1), 1–16. https://doi.org/10.1093/forestry/cpm032

Chen, G., Hay, G. J., Carvalho, L. M. T., & Wulder, M. A. (2012). Object-based change detection. *International Journal of Remote Sensing*, *33*(14), 4434–4457. https://doi.org/10.1080/01431161.2011.648285

Chen, J. M. (1996). Evaluation of Vegetation Indices and a Modified Simple Ratio for Boreal Applications. *Canadian Journal of Remote Sensing*, *22*(3), 229–242. https://doi.org/10.1080/07038992.1996.10855178

CyberTracker Conservation. (2013). CyberTracker GPS Field Data Collection System. Retrieved from http://www.cybertracker.org/

Daughtry, C. (2000). Estimating Corn Leaf Chlorophyll Concentration from Leaf and Canopy Reflectance. *Remote Sensing of Environment*, *74*(2), 229–239. https://doi.org/10.1016/S0034-4257(00)00113-

Doll, D. (2000). Statistiques historiques des grands chablis éoliens en Europe occidentale depuis le milieu du XIXe siècle: analyse critique. *Dossiers de l'Environnement de l'INRA*, *20*, 38–41.

Donat, M. G., Leckebusch, G. C., Wild, S., & Ulbrich, U. (2011). Future changes in European winter storm losses and extreme wind speeds inferred from GCM and RCM multi-model simulations. *Natural Hazards and Earth System Science*, *11*(5), 1351–1370. https://doi.org/10.5194/nhess-11-1351-2011

Dostálová, A., Hollaus, M., Milenković, M., & Wagner, W. (2016). Forest area derivation from Sentinel-1 data. *ISPRS Annals of Photogrammetry, Remote Sensing and Spatial Information Sciences*, *III-7*, 227–233. https://doi.org/10.5194/isprsannals-III-7-227-2016

Eitel, J. U. H., Vierling, L. A., Litvak, M. E., Long, D. S., Schulthess, U., Ager, A. A., … Stoscheck, L. (2011). Broadband, red-edge information from satellites improves early stress detection in a New Mexico conifer woodland. *Remote Sensing of Environment*, *115*(12), 3640–3646. https://doi.org/10.1016/j.rse.2011.09.002

European Space Agency. (2015). *Sentinel-2 User Handbook* (1.2). Retrieved from https://sentinels.copernicus.eu/web/sentinel/user-guides/document-library/-/asset_publisher/xlslt4309D5h/content/sentinel-2-user-handbook

European Space Agency. (2017). Sentinel-2 Toolbox. Retrieved from https://sentinel.esa.int/web/sentinel/toolboxes/sentinel-2

Evans, J. S., & Murphy, M. A. (2018). rfUtilities. Retrieved from https://cran.r-project.org/package=rfUtilities

Fernández-Manso, A., Fernández-Manso, O., & Quintano, C. (2016). SENTINEL-2A red-edge spectral indices suitability for discriminating burn severity. *International Journal of Applied Earth Observation and Geoinformation*, *50*, 170–175. https://doi.org/10.1016/j.jag.2016.03.005

Franklin, S., & Wulder, M. A. (2003). Remote sensing of forest environmnets, conclusions. Challenges and opportunities. In M. Wulder & S. Franklin (Eds.), *Remote Sensing of Forest Environments* (1st ed., pp. 511–514). Springer US. https://doi.org/10.1007/978-1-4615-0306-4

Genuer, R., Poggi, J.-M., & Malot, C. T.-. (2015). VSURF: An R Package for Variable Selection Using Random Forests. *The R Journal*, *7*(2), 19–33. Retrieved from https://journal.r-project.org/archive/2015/RJ-2015-018/index.html

Gitelson, A. A., & Merzlyak, M. N. (1998). Remote sensing of chlorophyll concentration in higher plant leaves. *Advances in Space Research*, *22*(5), 689–692. https://doi.org/10.1016/S0273-1177(97)01133-2

Gitelson, A., & Merzlyak, M. N. (1994). Spectral Reflectance Changes Associated with Autumn Senescence of Aesculus hippocastanum L. and Acer platanoides L. Leaves. Spectral Features and Relation to Chlorophyll Estimation. *Journal of Plant Physiology*, *143*(3), 286–292.

https://doi.org/10.1016/S0176-1617(11)81633-0

Google Earth Pro. (2018). Retrieved from https://www.google.com/earth/desktop/

GVA. (2017). Cartografía de montes gestionados por la GVA. Retrieved from http://catalogo.icv.gva.es/geonetwork/srv/spa/catalog.search#/metadata/spa_icv_fore_montes_gestionados

Haboudane, D., Miller, J. R., Pattey, E., Zarco-Tejada, P. J., & Strachan, I. B. (2004). Hyperspectral vegetation indices and novel algorithms for predicting green LAI of crop canopies: Modeling and validation in the context of precision agriculture. *Remote Sensing of Environment*, *90*(3), 337–352. https://doi.org/10.1016/j.rse.2003.12.013

Hardisky, M. A., Klemas, V., & Smart, R. M. (1983). The influence of soil salinity, growth form, and leaf moisture on the spectral radiance of Spartina alterniflora canopies. *Photogrammetric Engineering and Remote Sensing*, *49*(1), 77–83. Retrieved from https://www.asprs.org/wp-content/uploads/pers/1983journal/jan/1983_jan_77-83.pdf

Hawryło, P., Bednarz, B., Wężyk, P., & Szostak, M. (2018). Estimating defoliation of Scots pine stands using machine learning methods and vegetation indices of Sentinel-2. *European Journal of Remote Sensing*, *51*(1), 194–204. https://doi.org/10.1080/22797254.2017.1417745

Hijmans, R. J. (2017). raster: Geographic Data Analysis and Modeling. Retrieved from https://cran.r-project.org/package=raster

Hirschmugl, M., Gallaun, H., Dees, M., Datta, P., Deutscher, J., Koutsias, N., & Schardt, M. (2017). Methods for Mapping Forest Disturbance and Degradation from Optical Earth Observation Data: a Review. *Current Forestry Reports*, *3*(1), 32–45. https://doi.org/10.1007/s40725-017-0047-2

Holben, B. N. (1986). Characteristics of maximum-value composite images from temporal AVHRR data. *International Journal of Remote Sensing*, *7*(11), 1417–1434. https://doi.org/10.1080/01431168608948945

Huete, A. (1997). A comparison of vegetation indices over a global set of TM images for EOS-MODIS. *Remote Sensing of Environment*, *59*(3), 440–451. https://doi.org/10.1016/S0034-4257(96)00112-5

Huete, A., Didan, K., Miura, T., Rodriguez, E. ., Gao, X., & Ferreira, L. . (2002). Overview of the radiometric and biophysical performance of the MODIS vegetation indices. *Remote Sensing of Environment*, *83*(1–2), 195–213. https://doi.org/10.1016/S0034-4257(02)00096-2

Huete, A. R. (1988). A soil-adjusted vegetation index (SAVI). *Remote Sensing of Environment*, *25*(3), 295–309. https://doi.org/10.1016/0034-4257(88)90106-X

Hunt, E. R., Doraiswamy, P. C., McMurtrey, J. E., Daughtry, C. S. T., Perry, E. M., & Akhmedov, B. (2013). A visible band index for remote sensing leaf chlorophyll content at the canopy scale. *International Journal*

of Applied Earth Observation and Geoinformation, *21*, 103–112. https://doi.org/10.1016/j.jag.2012.07.020

Hunt Jr., E. R., & Rock, B. N. (1989). Detection of changes in leaf water content using Near- and Middle-Infrared reflectances☆. *Remote Sensing of Environment*, *30*(1), 43–54. https://doi.org/10.1016/0034-4257(89)90046-1

Hussain, M., Chen, D., Cheng, A., Wei, H., & Stanley, D. (2013). Change detection from remotely sensed images: From pixel-based to object-based approaches. *ISPRS Journal of Photogrammetry and Remote Sensing*, *80*, 91–106. https://doi.org/10.1016/j.isprsjprs.2013.03.006

Jiang, Z., Huete, A. R., Didan, K., & Miura, T. (2008). Development of a two-band enhanced vegetation index without a blue band. *Remote Sensing of Environment*, *112*(10), 3833–3845. https://doi.org/10.1016/j.rse.2008.06.006

Liaw, A., & Wiener, M. (2002). Classification and Regression by randomForest. *R News*, *2*(3), 18–22. Retrieved from http://cran.r-project.org/doc/Rnews/

Liberato, M. L. R. (2014). The 19 January 2013 windstorm over the North Atlantic: large-scale dynamics and impacts on Iberia. *Weather and Climate Extremes*, *5–6*, 16–28. https://doi.org/10.1016/j.wace.2014.06.002

Llasat, M. C., Turco, M., Quintana-Seguí, P., & Llasat-Botija, M. (2014). The snow storm of 8 March 2010 in Catalonia (Spain): a paradigmatic wet-snow event with a high societal impact. *Natural Hazards and Earth System Sciences*, *14*(2), 427–441. https://doi.org/10.5194/nhess-14-427-2014

MAGRAMA. (2015). Mapa Forestal de España 1:25.000.

Mallinis, G., Mitsopoulos, I., & Chrysafi, I. (2018). Evaluating and comparing Sentinel 2A and Landsat-8 Operational Land Imager (OLI) spectral indices for estimating fire severity in a Mediterranean pine ecosystem of Greece. *GIScience & Remote Sensing*, *55*(1), 1–18. https://doi.org/10.1080/15481603.2017.1354803

Martín-Alcón, S., Gil-Tena, A., & Cantón, J. (2017). *Delimitación y cuantificación de la biomasa forestal muerta en los bosques de la Comunitat Valenciana a partir del análisis de imágenes Sentinel-2 y LiDAR. Valencia*.

Martín-Alcón, S., González-Olabarría, J., & Coll, L. (2010). Wind and snow damage in the Pyrenees pine forests: effect of stand attributes and location. *Silva Fennica*, *44*(3). https://doi.org/10.14214/sf.138

Mašková, Z., Zemek, F., & Květ, J. (2008). Normalized difference vegetation index (NDVI) in the management of mountain meadows. *Boreal Environment Research*, *13*, 417–432.

Miller, J. D., & Thode, A. E. (2007). Quantifying burn severity in a heterogeneous landscape with a relative

version of the delta Normalized Burn Ratio (dNBR). *Remote Sensing of Environment*, *109*(1), 66–80.

Montagné-Huck, C., & Brunette, M. (2018). Economic analysis of natural forest disturbances: A century of research. *Journal of Forest Economics*, *32*, 42–71. https://doi.org/10.1016/j.jfe.2018.03.002

Nielsen, A. A. (2007). The Regularized Iteratively Reweighted MAD Method for Change Detection in Multi- and Hyperspectral Data. *IEEE Transactions on Image Processing*, *16*(2), 463–478. https://doi.org/10.1109/TIP.2006.888195

Núñez Mora, J. Á. (2017). El temporal del 17 al 23 de enero de 2017 en la Comunidad Valenciana - Revista del Aficionado a la Meteorología. Retrieved from https://www.tiempo.com/ram/310202/el-temporal-del-17-al-23-de-enero-de-2017-en-la-comunidad-valenciana/

Nykänen, M.-L., Peltola, H., Quine, C. P., Kellomäki, S., & Broadgate, M. (1997). Factors affecting snow damage of trees with particular reference to European conditions. *Silva Fennica*, *31*(2), 193–213. Retrieved from https://helda.helsinki.fi/handle/1975/8519

Pickett, S. T. A., Kolasa, J., Armesto, J. J., & Collins, S. L. (1989). The Ecological Concept of Disturbance and Its Expression at Various Hierarchical Levels. *Oikos*, *54*(2), 129. https://doi.org/10.2307/3565258

QGIS Development Team. (2018). QGIS Geographic Information System. Open Source Geospatial Foundation Project. Retrieved from http://qgis.osgeo.org

Qi, J., Chehbouni, A., Huete, A. R., Kerr, Y. H., & Sorooshian, S. (1994). A modified soil adjusted vegetation index. *Remote Sensing of Environment*, *48*(2), 119–126. https://doi.org/10.1016/0034-4257(94)90134-1

Ramoino, F., Tutunaru, F., Pera, F., & Arino, O. (2017). Ten-Meter Sentinel-2A Cloud-Free Composite—Southern Africa 2016. *Remote Sensing*, *9*(7), 652. https://doi.org/10.3390/rs9070652

Riano, D., Chuvieco, E., Salas, J., & Aguado, I. (2003). Assessment of different topographic corrections in landsat-TM data for mapping vegetation types (2003). *IEEE Transactions on Geoscience and Remote Sensing*, *41*(5), 1056–1061. https://doi.org/10.1109/TGRS.2003.811693

Rondeaux, G., Steven, M., & Baret, F. (1996). Optimization of soil-adjusted vegetation indices. *Remote Sensing of Environment*, *55*(2), 95–107. https://doi.org/10.1016/0034-4257(95)00186-7

Rouse, J. W., Haas, R. H., Schell, J. A., & Deering, D. W. (1974). Monitoring vegetation systems in the Great Plains with ERTS. In *NASA Goddard Space Flight Center 3d ERTS-1 Symposium* (pp. 309–317). Retrieved from https://ntrs.nasa.gov/search.jsp?R=19740022614

RStudio Team. (2016). RStudio: Integrated Development Environment for R. Boston, MA. Retrieved from http://www.rstudio.com/

Schelhaas, M.-J., Nabuurs, G.-J., & Schuck, A. (2003). Natural disturbances in the European forests in the

19th and 20th centuries. *Global Change Biology*, *9*(11), 1620–1633. https://doi.org/10.1046/j.1365-2486.2003.00684.x

Schroeder, T. A., Schleeweis, K. G., Moisen, G. G., Toney, C., Cohen, W. B., Freeman, E. A., … Huang, C. (2017). Testing a Landsat-based approach for mapping disturbance causality in U.S. forests. *Remote Sensing of Environment*, *195*, 230–243. https://doi.org/10.1016/j.rse.2017.03.033

Schultz, M., Clevers, J. G. P. W., Carter, S., Verbesselt, J., Avitabile, V., Quang, H. V., & Herold, M. (2016). Performance of vegetation indices from Landsat time series in deforestation monitoring. *International Journal of Applied Earth Observation and Geoinformation*, *52*, 318–327. https://doi.org/10.1016/j.jag.2016.06.020

Sripada, R. P., Heiniger, R. W., White, J. G., & Meijer, A. D. (2006). Aerial Color Infrared Photography for Determining Early In-Season Nitrogen Requirements in Corn. *Agronomy Journal*, *98*(4), 968. https://doi.org/10.2134/agronj2005.0200

Tucker, C. J. (1979). Red and photographic infrared linear combinations for monitoring vegetation. *Remote Sensing of Environment*, *8*(2), 127–150. https://doi.org/10.1016/0034-4257(79)90013-0

Verhegghen, A., Eva, H., Ceccherini, G., Achard, F., Gond, V., Gourlet-Fleury, S., & Cerutti, P. O. (2016). The potential of sentinel satellites for burnt area mapping and monitoring in the Congo Basin forests. *Remote Sensing*, *8*(12), 1–22. https://doi.org/10.3390/rs8120986

Wang, W., Qu, J. J., Hao, X., Liu, Y., & Stanturf, J. A. (2010). Post-hurricane forest damage assessment using satellite remote sensing. *Agricultural and Forest Meteorology*, *150*(1), 122–132. https://doi.org/10.1016/j.agrformet.2009.09.009

Welikhe, P., Quansah, J. E., Fall, S., & McElhenney, W. (2017). Estimation of Soil Moisture Percentage Using LANDSAT-based Moisture Stress Index. *Journal of Remote Sensing & GIS*, *06*(02). https://doi.org/10.4172/2469-4134.1000200

White, P. S., & Pickett, S. T. A. (1985). Natural Disturbance and Patch Dynamics: An Introduction. In *The Ecology of Natural Disturbance and Patch Dynamics* (pp. 3–13). Elsevier. https://doi.org/10.1016/B978-0-12-554520-4.50006-X

Wu, J., Wang, T., Pan, K., Li, W., & Huang, X. (2016). Assessment of forest damage caused by an ice storm using multi-temporal remote-sensing images: a case study from Guangdong Province. *International Journal of Remote Sensing*, *37*(13), 3125–3142. https://doi.org/10.1080/01431161.2016.1194544